Electronic Supplementary Material (ESI) for Sustainable Energy & Fuels.

Supporting information

Dendrite-free deposition and side-reaction suppression of zinc anodes achieved via constructing synergistic interface buffer layers

Ting Li[a,#], Bo Zhou[a,c,#], Zhongfu Yan[a,#], Anjun Hu[a,b,*], Mengjiao Liu[a], Xinyu Liu[a], Liang Liu[c,*], Miao He[a,d], Jiahao Chen[a], Jianping Long[a,*]

[a] College of Materials and Chemistry & Chemical Engineering, Chengdu University of Technology, 1#, Dongsanlu, Erxianqiao, Chengdu 610059, Sichuan, P. R. China

[b] College of Computer Science and Cyber Security, Chengdu University of Technology, 1#, Dongsanlu, Erxianqiao, Chengdu 610059, Sichuan, P. R. China

[c] Zhangjiajie Institute of Aeronautical Engineering, 1#, xueyuan Rd, Wulingshan Avenue, Zhangjiajie 427000, Hunan, P. R. China

[d] State Key Laboratory of Electronic Thin Film and Integrated Devices, University of Electronic Science and Technology of China, Chengdu, 610054, China

[#] These authors contributed to this work equally.

*Corresponding author: anjunhu@cdut.edu.cn (Anjun Hu); xiaopengliuliang@163.com (Liang Liu); longjianping@cdut.cn (Jianping Long)

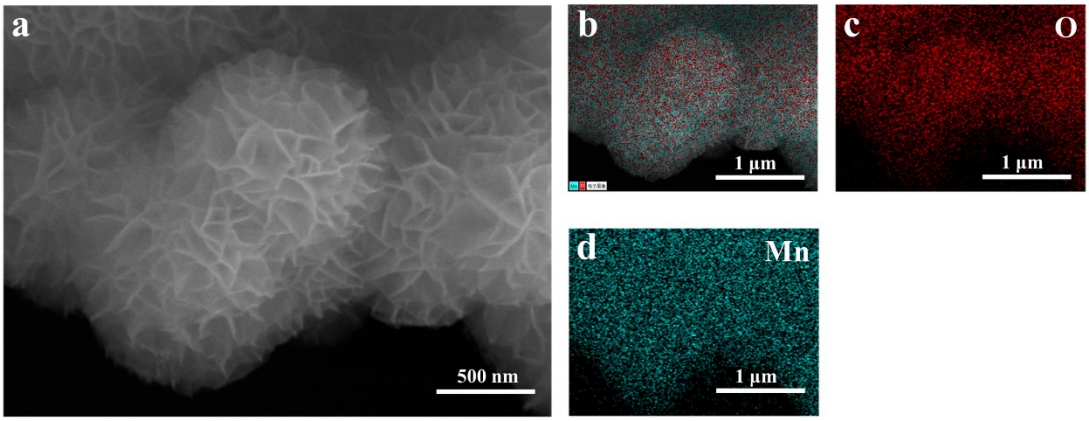

Figure S1. Corresponding O and Mn elemental mapping images of δ-MnO_2 samples.

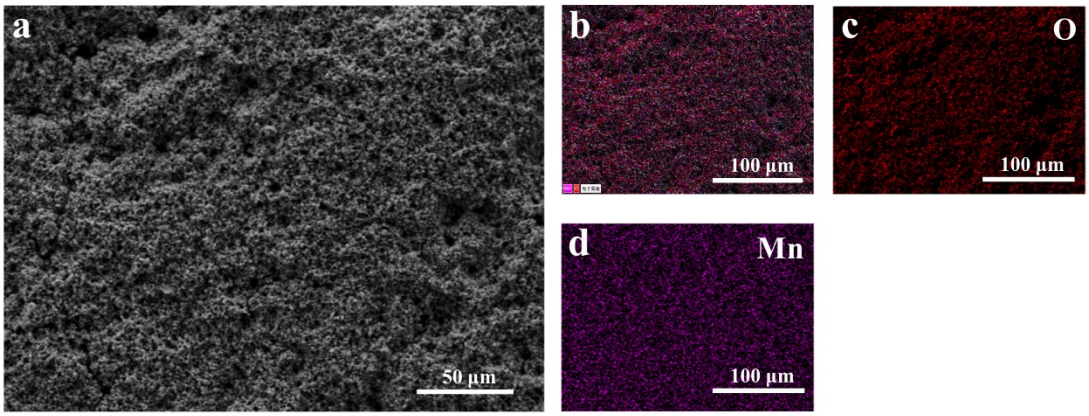

Figure S2. Corresponding O and Mn elemental mapping images of δ-MnO_2@Zn.

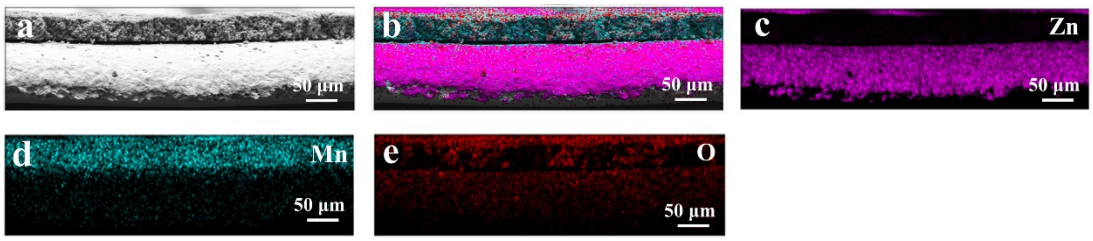

Figure S3. Cross-sectional O and Mn elemental mapping images of δ-MnO_2@Zn.

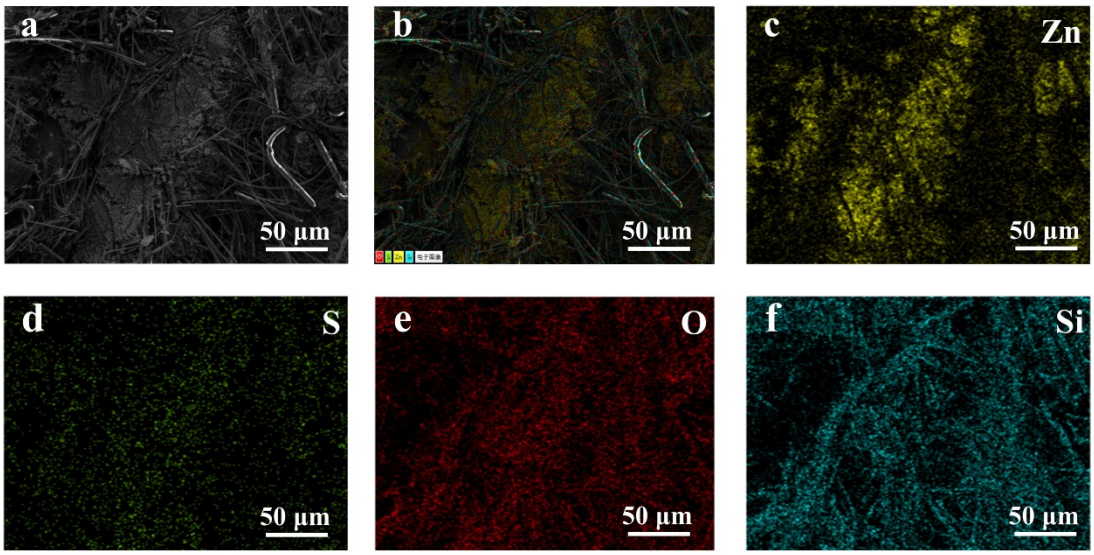

Figure S4. Corresponding Zn, S, O and Si elemental mapping images of bare Zn after plating at 0.25 mA cm^{-2} and 0.5 mAh cm^{-2}.

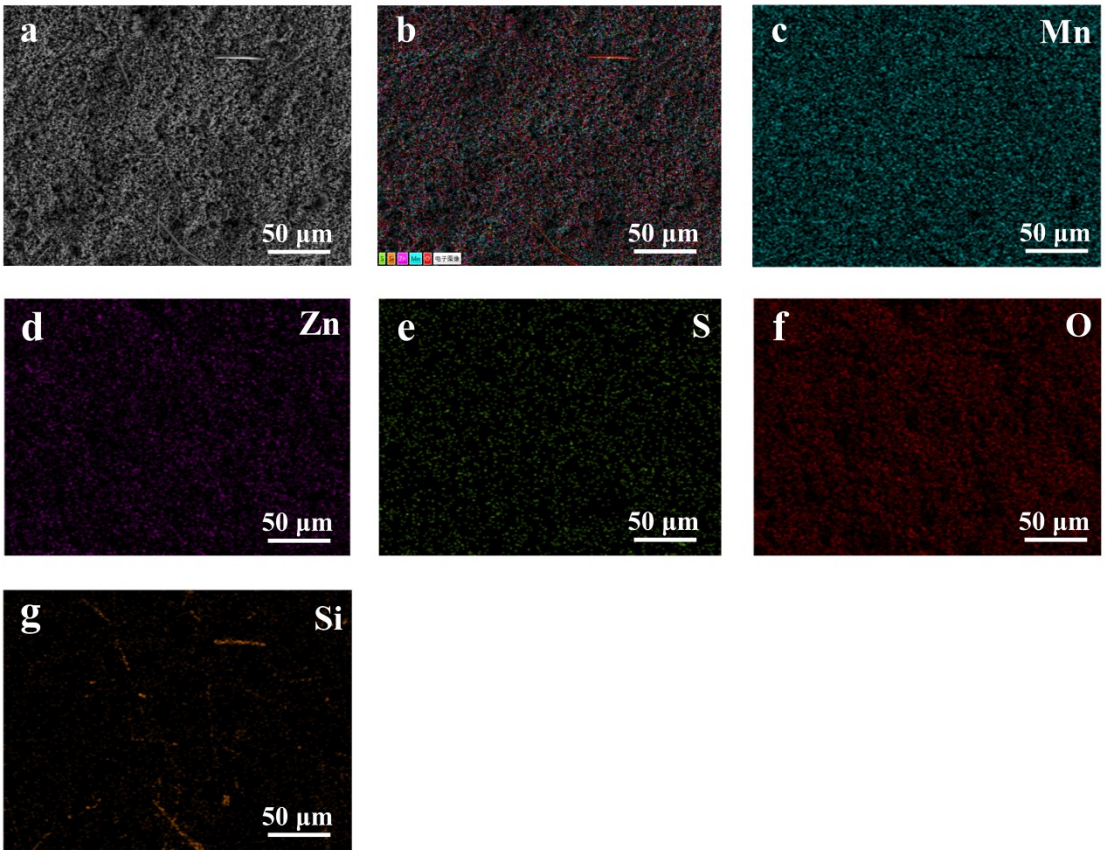

Figure S5. Corresponding Mn, Zn, S, O and Si elemental mapping images of δ-MnO_2@Zn after plating at 0.25 mA cm^{-2} and 0.5 mAh cm^{-2}.

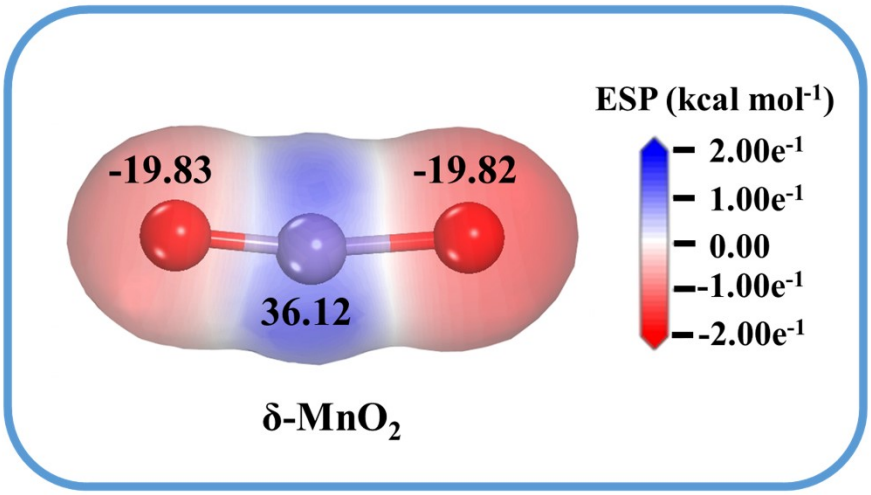

Figure S6. Electrostatic potential on van der Waals surfaces δ-MnO_2.

Supporting Note: limit element analysis (FEM) conducted by COMSOL Multiphysics has been used to investigate the distribution of Zn^{2+} through our structure. The migration of Zn^{2+}driven by electric field and diffusion flow in both liquid phase (electrolytes) and solid phase was considered in these simplified simulations. Two physical models of electrostatic and transport of diluted species based on the partial differential equations listed below were coupled to conduct FEM simulation. [1-2]

$$E = -\nabla\phi$$
$$N = -D\nabla = c + ucE$$
$$\frac{\partial c}{\partial t} = -\nabla N$$

where ϕ is the electric potential, E is the electric field, D is the diffusion coefficient of Zn^{2+}, c is the concentration of Zn^{2+}, u is the ionic mobility of $Zn^{2+`}$ in electrolytes, and N is the flux vector of Zn^{2+}, t is the diffusion time. These FEM simulations on the routine our composite separator was performed in a rectangle area, respectively. The potential difference Δϕ through these electrolytes was set as 10 mV. To investigate the ion transport behaviors with limited liquid electrolytes in long time cycling, the same physical model was established and the ratio of diffusion coefficients of Zn^{2+} in liquid electrolytes and solid particles was decreased to 8.0. The mobilities of Zn^{2+} for liquid electrolyte and solid particles are defined by the Nernst-Einstein equation. The bottom boundaries of two simulation areas are the Dirichlet boundaries with ϕ_0 = 0 V and c_0 = 0 M. The top boundaries of two simulation area are also Dirichlet boundaries with ϕ1 = 20 mV and

c1 = 1.0 M. The other boundaries are natural boundaries with zero flux.

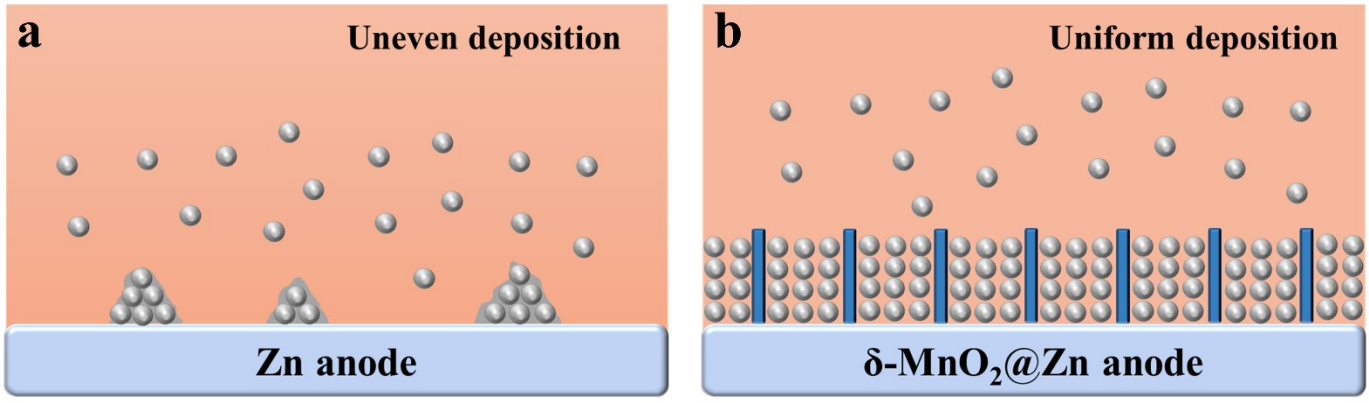

Figure S7. Schematic images of the Zn deposition process on (a) bare Zn and (b) δ-MnO_2@Zn anodes.

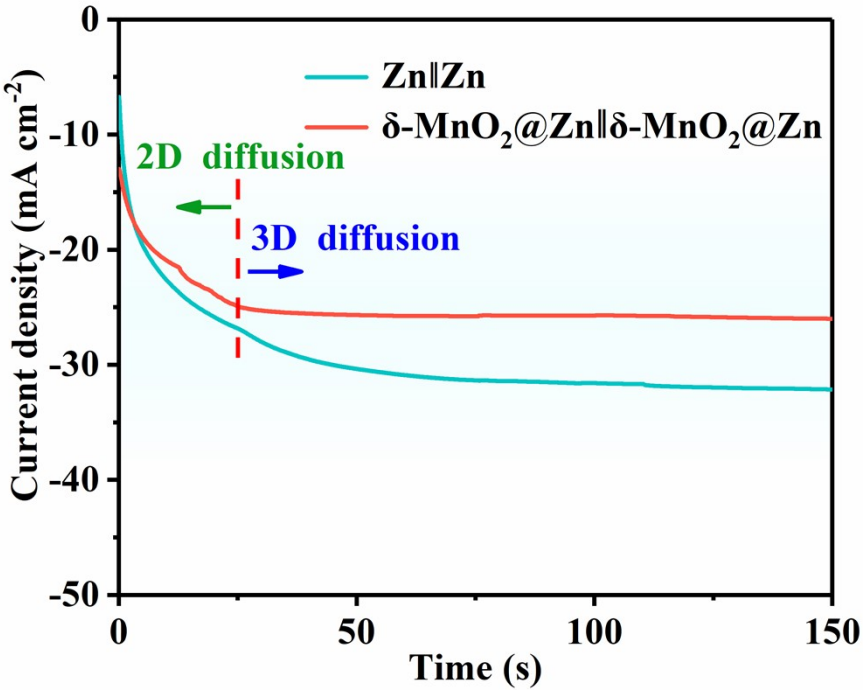

Figure S8. Chronoamperometry (CA) at -200 mV of overpotential and the corresponding illustration of the Zn^{2+} diffusion and reduction processes for bare Zn and δ-MnO_2@Zn anodes.

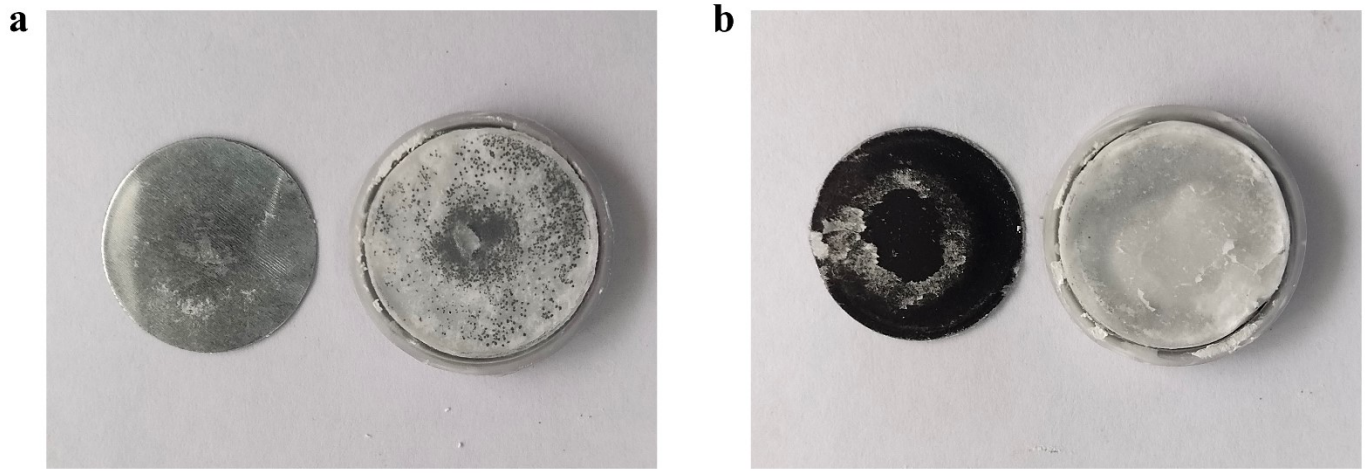

Figure S9. Photographs of (a) bare Zn and (b) δ-MnO_2@Zn electrodes after 10 cycles at 3 mA cm^{-2} and 1.5 mAh cm^{-2}.

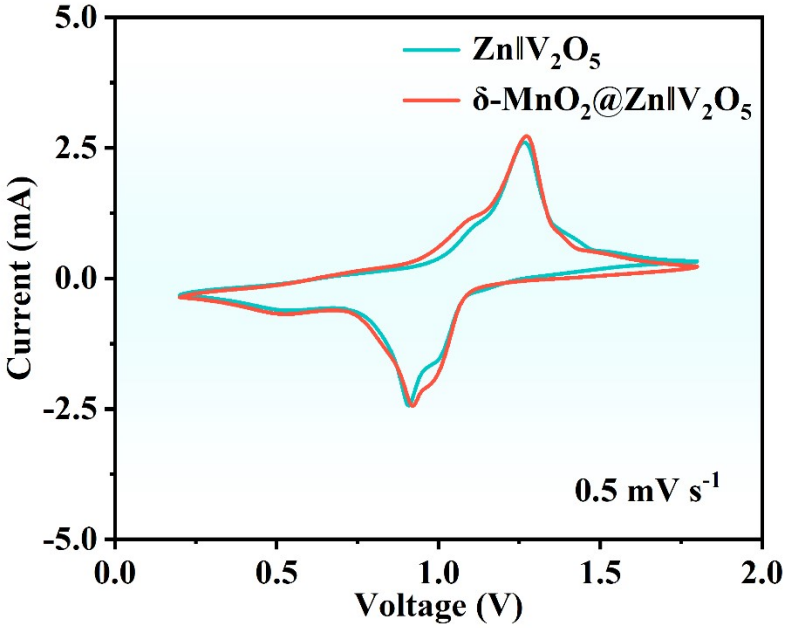

Figure S10. CV curves of Zn‖V_2O_5 and δ-MnO_2@Zn‖V_2O_5 cells at 0.5 mV s^{-1}.

Supplementary Table

Table S1. Comparison of main parameters and cycling property for this work with recently reported Zn-based symmetrical cells.

Interfacial layer	Current density (mA cm^{-2})	Capacity (mAh cm^{-2})	Life (h)	Reference
rGO	1	1	300	[3]
$CaCO_3$	1	0.05	836	[4]
Carbon	1	1	200	[5]
TiO_2	1	1	480	[6]
PSN	1	1	800	[7]
Mxene	0.2	0.2	820	[8]
PAN	0.5	0.25	350	[9]
δ-MnO_2	**1**	**0.5**	**890**	**This work**

References

[1] J. Newman, K.E. Thomas, H. Hafezi, D.R. Wheeler, *J. Power Sources*, 2003, **119**, 838. https://doi.org/10.1016/S0378-7753(03)00282-9.

[2] K.E. Thomas-Alyea, J. Newman, G. Chen, T.J. Richardson, *J. Electrochem. Soc.*, 2004, **151**, A509. https://doi.org/10.1149/1.1649232.

[3] A. Xia, X. Pu, Y. Tao, H. Liu, Y. Wang, *Appl. Surf. Sci.*, 2019, **481**, 852. https://doi.org/10.1016/j.apsusc.2019.03.197.

[4] L. Kang, M. Cui, F. Jiang, Y. Gao, H. Luo, J. Liu, W. Liang, C. Zhi, *Adv. Energy Mater.*, 2018, ***8***, 1801090. https://doi.org/10.1002/aenm.201801090.

[5] W. Li, K. Wang, M. Zhou, H. Zhan, S. Cheng, K. Jiang, *ACS Appl. Mater. Interfaces*, 2018, **10**, 22059. https://doi.org/10.1021/acsami.8b04085.

[6] Q. Zhang, J. Luan, X. Huang, Q. Wang, D. Sun, Y. Tang, X. Ji, H. Wang, *Nat. Commun.*, 2020, **11**, 3961. https://doi.org/10.1038/s41467-020-17752-x.

[7] S. Zhou, Y. Wang, H. Lu, Y. Zhang, C. Fu, I. Usman, Z. Liu, M. Feng, G. Fang, X. Cao, *Adv. Funct. Mater.*, 2021, **31**, 2104361. https://doi.org/10.1002/adfm.202104361.

[8] N. Zhang, S. Huang, Z. Yuan, J. Zhu, Z. Zhao, Z. Niu, *Angew. Chem. Int. Ed.*, 2021, **133**, 2897. https://doi.org/10.1002/anie.202012322.

[9] B.-S. Lee, S. Cui, X. Xing, H. Liu, X. Yue, V. Petrova, H.-D. Lim, R. Chen, P. Liu, *ACS Appl. Mater. Interfaces*, 2018, **10**, 38928. https://doi.org/10.1021/acsami.8b14022.